Proceedings of 5th Jagiellonian Symposium on Advances in Particle Physics and Medicine, Kraków, Poland, 2024

Calculational Cross-Sections of (p, x) Reactions on the ^{12}C, ^{14}N and ^{16}O for ^{10,11}C Production

N. Sakhno[a,b,*], W. Mryka[c,d], O. Gorbachenko[b], I. Kadenko[a,b], E. Stępień[c,d] and P. Moskal[c,d]

[a] *International Nuclear Safety Center of Ukraine, Taras Shevchenko National University of Kyiv, St. Volodymyrska 64/13, 01601 Kyiv, Ukraine*
[b] *Department of Nuclear and High Energy Physics, Faculty of Physics, Taras Shevchenko National University of Kyiv, St. Volodymyrska 64/13, 01601 Kyiv, Ukraine*
[c] *Faculty of Physics, Astronomy and Applied Computer Science, Jagiellonian University, Kraków, Poland*
[d] *Center for Theranostics, Jagiellonian University, Kraków, Poland*

Doi: 10.12693/APhysPolA.146.731 *e-mail: nadiia.sakhno@knu.ua

For *in vivo* dose delivery monitoring in proton therapy the positron emission tomography can be applied because the positron emitters are being produced by the nuclear reactions of protons with atomic nuclei in a human body. The estimation of cross-sections of proton-induced nuclear reactions in the body is, therefore, one of the important steps on the way to develop proton beam range monitoring with positron emission tomography. Here, we calculate cross-sections for all open nuclear reaction channels initiated by 150 MeV protons and featured with ^{10}C and ^{11}C formation in the output channels. Taking into account the composition of elements in the human body and the data from the literature, we estimated ^{10}C and ^{11}C cumulative production cross-sections for proton-induced reactions in the human body.

topics: short-lived carbon isotopes, proton-induced nuclear reactions, positron emission tomography, dose delivery validation

1. Introduction

One of the most promising methods for *in vivo* radiation dose delivery validation in proton beam therapy is positron emission tomography (PET) [1–9]. Correct estimations of the produced PET radioisotopes during proton irradiations can be the basis for evaluating the correct *in vivo* dose delivery and controling the location of the dose delivery. For a proton beam of 150 MeV energy, many nuclear reaction channels are open and contribute towards the production of short-lived nuclides. The produced isotopes emitting positrons are for example: ^{11}C, ^{10}C, ^{14}O, ^{15}O, ^{13}N, ^{30}P, ^{38}K [10–14].

The carbon isotopes ^{10}C and ^{11}C can be produced in (p, x) reactions on ^{12}C, ^{14}N and ^{16}O. In order to calculate the cross-section for these reactions as a function of the proton energy, we apply the TALYS-2.0 [3] code using a two-component exciting model to describe the pre-equilibrium processes and the equilibrium state according to the Hauser–Feshbach model with a deformed optical potential. We compare the results of the cross-section calculations with experimental data from available nuclear data libraries and cross-sections determined with other models [12–14].

2. Reactions

In our study, we considered only proton-induced reactions on the main chemical elements of the human body: carbon, nitrogen and oxygen, in particular on their most abundant isotopes: ^{12}C, ^{14}N and ^{16}O, with the formation of ^{10}C and ^{11}C in the output channels. The isotope ^{10}C has the half-life of 19.309 s and decays only via the electron capture (EC) or positron emission (β^+) mode; the reaction is: $^{10}\mathrm{C} \rightarrow {}^{10}\mathrm{B}^* + e^+ + \nu_e \rightarrow {}^{10}\mathrm{B} + \gamma\,(718\,\mathrm{keV}) + \mathrm{e}^+ + \nu_\mathrm{e}$. The ^{11}C isotope possess the half-life of 20.364 m and decays via the reaction: $^{11}\mathrm{C} \rightarrow {}^{11}\mathrm{B} + e^+ + \nu_e$. Both of the mentioned isotopes emit positrons and can be used for beam range monitoring. The fact that ^{10}C emits additional prompt gamma opens the possibility for positronium imaging during the proton therapy [1, 15–17], as well as for disentangling signals from different isotopes [18, 19]. Simultaneous registration of annihilation photons and prompt gamma become possible with the recently demonstrated multiphoton PET tomography systems [20–23]. Using multiphoton Jagiellonian PET (J-PET) system, the first *in-vivo* positronium images of humans were recently demonstrated [24], and also first phantom studies with clinical PET

TABLE I

Kinematic data for 150 MeV proton energy of incident protons of the $^{12}C(p,x)^{10,11}C$ reactions.

Reaction products	Q-value [keV]	Threshold [keV]
$^{11}C + d$	−16496.12(6)	17882.12(7)
$^{11}C + NN + p$	−18720.69(6)	20293.60(7)
$^{10}C + t$	−23359.48(7)	25322.15(8)
$^{10}C + NN + d$	−29616.71(7)	32105.11(8)
$^{10}C + 2NN + p$	−31841.28(7)	34516.58(8)

system were reported [25]. It was also shown that positronium is a promising biomarker of tissue pathology [26–29] and a possible biomarker of hypoxia [30–32]. The possibility of hypoxia assessment during irradiation with the proton beam would be beneficial for the proper effective planning of the tumor treatment [1].

2.1. Proton-induced nuclear reaction channels on ^{12}C with production of $^{10,11}C$ in the output channel

The kinematic data about these reactions $^{12}C+p$ ($E_{lab} = 150\,000$ keV) are presented in Table I as an example. In the table, the Q-value denotes the energetic balance of the reaction (energy release or absorption). The production of $^{10,11}C$ in $^{12}C(p,x)$ nuclear reaction was investigated up to 150 MeV of proton impinging energy. Graphical representation of the calculation results obtained using TALYS-2.0 code are given in Figs. 1 and 2. The data are taken from the EXFOR [12], JENDL-5.0 [13], and ENDF/B-VIII [14] libraries, as well as TALYS calculations. The experimental data is taken from the EXFOR data library, and the figures presented indicate this experimental data with the corresponding reference to the year of publications, first author and EXFOR-ID subentry number with a brief description of the experimental technique, as can be seen at the EXFOR site [12]. The cross-section for the production of ^{11}C is expected to be greater than the one for ^{10}C. The obtained TALYS predictions underestimate the available experimental results.

2.2. Proton-induced nuclear reaction channels on ^{14}N with production of $^{10,11}C$ in the output channel

The production of $^{10,11}C$ in $^{14}N(p,x)$ nuclear reactions was also investigated up to 150 MeV of proton-impinging energy. Graphical representation of the calculation results based on the TALYS-2.0 code is shown in Figs. 3 and 4. Other data is

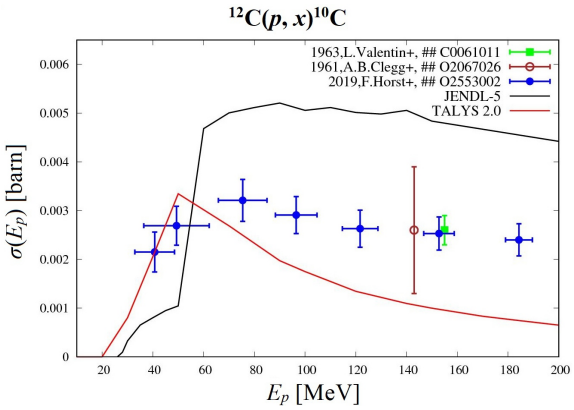

Fig. 1. Calculation results for the $^{12}C(p,x)^{10}C$ nuclear reaction.

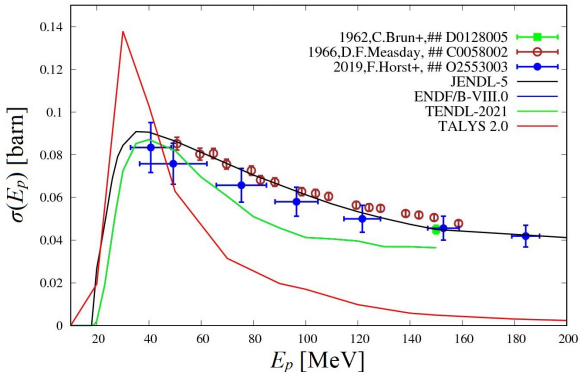

Fig. 2. Calculation results for the $^{12}C(p,x)^{11}C$ nuclear reaction.

taken from the EXFOR and JENDL-5 libraries. The cross-sections are quite low, the experimental data are scarce, and even the trends with respect to the energy predicted are quite different between the calculated, evaluated and poorly available experimental data. From these data analysis, it would be rather justified to rely on the TALYS results as they are closer to fewer experimental measurements. However, a potential discrepancy in two times between the JENDL and TALYS data for proton energies above 100 MeV in the case of ^{10}C can be taken into account.

2.3. Proton-induced reaction channels on ^{16}O with production of $^{10,11}C$ in the output channel

The production of $^{10,11}C$ in $^{16}O(p,x)$ nuclear reactions was also investigated up to 150 MeV of proton-impinging energy. Some experimental data is available, which creates the basis for a much better theoretical description and validation. A graphic representation of the calculation results is shown in Figs. 5 and 6, based on the TALYS-2.0 code output files.

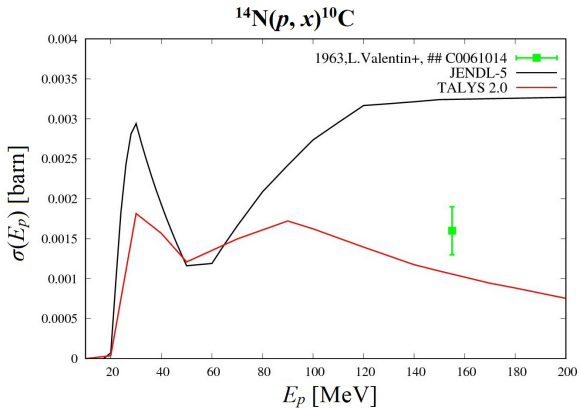

Fig. 3. Calculation results for the $^{14}\mathrm{N}(p,x)^{10}\mathrm{C}$ nuclear reaction.

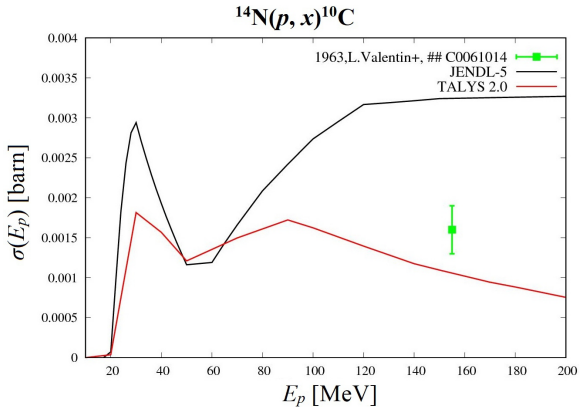

Fig. 4. Calculation results for the $^{14}\mathrm{N}(p,x)^{11}\mathrm{C}$ nuclear reaction.

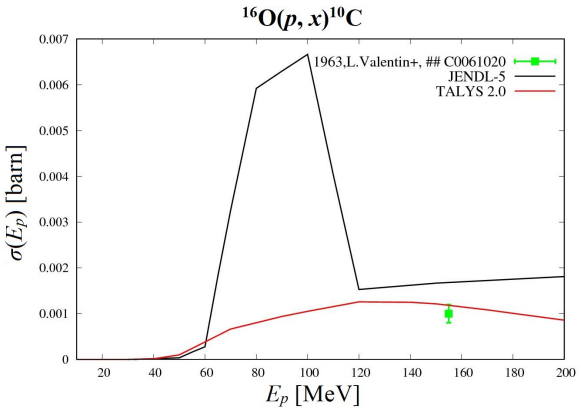

Fig. 5. Calculation results for the $^{16}\mathrm{O}(p,x)^{10}\mathrm{C}$ nuclear reaction.

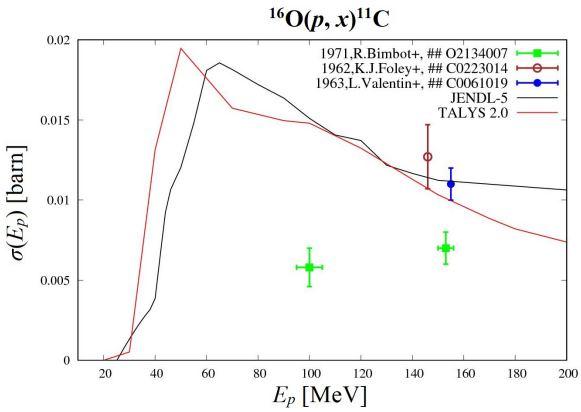

Fig. 6. Calculation results for the $^{16}\mathrm{O}(p,x)^{11}\mathrm{C}$ nuclear reaction.

Data is also taken from EXFOR and JENDL-5 libraries. There is a good correspondence between some experimental, evaluated and calculated data for ^{11}C production. Again, the cross-section of ^{11}C production is expected to be greater than for ^{10}C and this is confirmed by the experimental result. According to JENDL-5, the production of ^{10}C must be significantly greater in the energy range from 60 to 120 MeV, but this irregularity is not confirmed by any experimental data yet. At the same time, this feature must be kept in mind in case of unclear experimental results for this proton energy range.

3. Cumulative production of ^{10,11}C nuclei in the human body

For *in vivo* radiation dose delivery validation, we have to clearly realize that the PET image will reflect an integrated picture of the ^{10,11}C production.

Then, taking into account the atomic composition of the human body and the ratios of the ^{12}C, ^{14}N and ^{16}O isotopes concentration relative to the total number of atoms, $k_i = n_i/n_{\mathrm{atom}}$ (k_i — concentrations of the ^{12}C, ^{14}N, ^{16}O isotopes in the human body, i.e., $k_{^{16}\mathrm{O}} = 0.24$, $k_{^{12}\mathrm{C}} = 0.12$, $k_{^{14}\mathrm{N}} = 0.011$) and using the following normalisation

$$\omega_i = \frac{k_i}{\sum\limits_{i=^{12}\mathrm{C},^{14}\mathrm{N},^{16}\mathrm{O}} k_i}, \tag{1}$$

with $\omega_{^{16}\mathrm{O}} = 0.647$, $\omega_{^{12}\mathrm{C}} = 0.323$, $\omega_{^{14}\mathrm{N}} = 0.0296$, one can define the full weighted relative cross-section of ^{10}C and the production of ^{11}C as follows

$$\sigma_{\mathrm{tot}} = \sum_{i=^{12}\mathrm{C},^{14}\mathrm{N},^{16}\mathrm{O}} \omega_i\, \sigma_i. \tag{2}$$

The production rates R [s^{-1}] for the ^{10,11}C isotopes are defined as follows

$$R = \sigma_{\mathrm{tot}} \sum_{i=^{12}\mathrm{C},^{14}\mathrm{N},^{16}\mathrm{O}} k_i\, n_{\mathrm{atom}}\, j, \tag{3}$$

where j [cm^{-2}s^{-1}] — the flux density of protons in the human body.

When we look at the production of the PET radioactive isotopes ^{10}C, ^{11}C, they can be generated in different ways. We used the relative ω_i constants to distinguish which of the isotopes ^{12}C, ^{14}N, ^{16}O contribute towards the ^{10}C and ^{11}C isotopes in

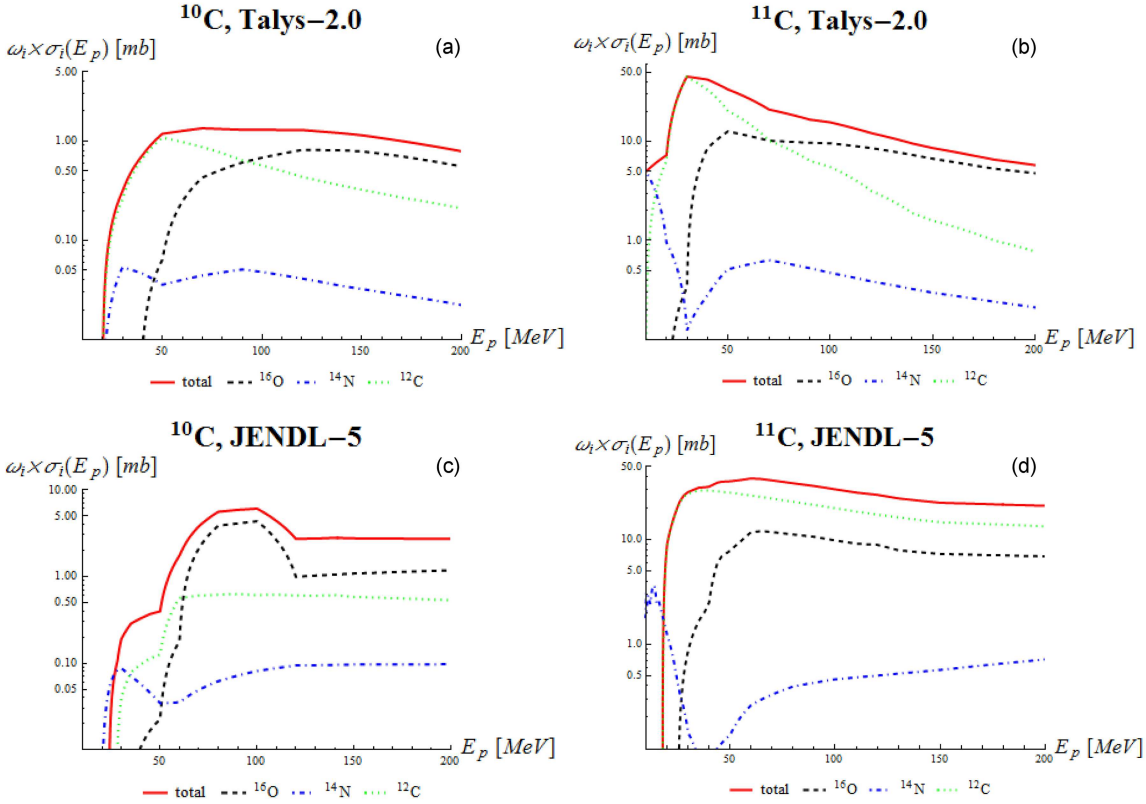

Fig. 7. Comparison of the ^{10}C and ^{11}C cumulative production reaction cross-section based on TALYS-2.0 code and JENDL-5 data.

the (p, x) reactions more effectively, with account of their concentrations in the human body. The ω_i's are relative and normalized to unity concentrations of ^{12}C, ^{14}N, ^{16}O isotopes, and the product $= \omega_i\, \sigma_i$ indicates the relative efficiency of the production rate of the isotopes ^{10}C, ^{11}C from one of the i-isotopes: ^{12}C, ^{14}N, ^{16}O.

Then we performed the calculations to compare the ^{10}C and ^{11}C cumulative production reaction cross-sections, and the data are now shown in Fig. 7.

As a result, there is an essential difference between TALYS-2.0 and JENDL-5 data.

All the presented cross-sections for the ^{10,11}C production are available in the Jagiellonian University Repository, see [33].

Cross-sections for the ^{14,15}O production, published in the recent article [34], are also available in the Jagiellonian University Repository [35].

4. Conclusions

In our study, we calculated the proton-induced nuclear reaction cross-sections on the stable isotopes ^{12}C, ^{14}N, and ^{16}O that are the major components of the human body, leading to the formation of ^{10}C and ^{11}C as reaction products. For all these isotopes, the formation of ^{11}C dominates over the formation of ^{10}C. This means that PET images will mainly reflect information about the ^{11}C formation and further decay. However, the presence of ^{10}C due to the emission of prompt gamma may enable the developpment of the *in-vivo* assessment of hypoxia based on the possibility of positronium imaging [17, 24, 30].

When considering the cumulative production of ^{10}C and ^{11}C in a human body, the major contribution to the ^{10}C cumulative production is due to proton-induces nuclear reactions on ^{16}O and ^{12}C isotopes, while the contribution from ^{14}N is much lower. For ^{11}C, the main contribution to the cumulative production is also due to reactions on ^{12}C and ^{16}O, but according to TALYS calculations, the cross-section of nuclear reactions on ^{16}O is greater, and on ^{12}C — lower. At the same time, according to JENDL-5, the situation is opposite, i.e., the cross-section on ^{12}C is greater, and on ^{16}O — lesser. Which of the results is correct it is unclear and requires separate and very thorough studying due to the scarcity of experimental data. As for now, for ^{16}O the JENDL-5 data is more trustworthy, and for ^{12}C — the TALYS data, as can be seen in Figs. 2 and 6. Taking into account a relative content of ^{12}C, ^{14}N and ^{16}O in the human body, the reaction yield for ^{10}C is expected to be lower than for ^{11}C by one order of magnitude.

Acknowledgments

This work was supported by the Foundation for Polish Science through the TEAM POIR.04.04.00-00-4204/17 program, by the National Science Centre through grants nos.: 2021/42/A/ST2/00423, 2021/43/B/ST2/02150, 2022/47/I/NZ7/03112, the Ministry of Education and Science through grant no. SPUB/SP/490528/2021, and the SciMat and qLife Priority Research Areas budget under the program Excellence Initiative–Research University at the Jagiellonian University.

References

[1] K. Parodi, T. Yamaya, P. Moskal, *Z. Med. Phys.* **33**, 22, (2023).

[2] C. Graeff, L. Volz, M. Durante, *Prog. Part. Nucl. Phys.* **131**, 104046 (2023).

[3] M. Durante, R. Orecchia, J.S. Loeffler, *Nat. Rev. Clin. Oncol.* **14**, 483 (2017).

[4] K. Brzeziński, J. Baran, D. Borys et al., *Phys. Med. Biol.* **68**, 145016 (2023).

[5] M. Durante, J.S. Loeffler, *Nat. Rev. Clin Oncol.* **7**, 37 (2010).

[6] K. Lang, *Bio-Algorithms Med-Syst.* **18**, 96 (2022).

[7] F. Abouzahr, J.P. Cesar, P. Crespoet et al., *Phys. Med. Biol.* **68**, 125001 (2023).

[8] F. Abouzahr, J.P. Cesar, P. Crespo et al., *Phys. Med. Biol.* **68**, 235004 (2023).

[9] S. Purushothaman, D. Kostyleva, P. Dendooven et al., *Sci. Rep.* **13**, 18788 (2023) .

[10] W. Mryka, M. Das, E.Y. Beyene, P. Moskal, E. Stępień, *Bio-Algorithms Med-Syst.* **19**, 96 (2023).

[11] A.J. Koning, D. Rochman, *Nucl. Data Sheets* **113**, 2841 (2012).

[12] National Nuclear Data Center (NNDC), Experimental Nuclear Reaction Data (EXFOR), 2024.

[13] Nuclear Data Center, Japan Atomoic Energy Agency (JAEA), JENDL-5, 2023.

[14] National Nuclear Data Center (NNDC), ENDF/B-VIII.0 Evaluated Nuclear Data Library, 2018.

[15] P. Moskal, in: 2019 IEEE Nuclear Science Symp. and Medical Imaging Conf. (NSS/MIC), Manchester, IEEE, 2020.

[16] P. Moskal, D. Kisielewska, C. Curceanu et al. *Phys. Med. Biol.* **64**, 055017 (2019).

[17] P. Moskal, K. Dulski, N. Chug et al., *Sci. Adv.* **7**, eabh4394 (2021).

[18] E. Beyene, M. Das, M Durak-Kozica et al., *Bio-Algorithms Med-Syst.* **19**, 101 (2023).

[19] M. Das, W. Mryka, E. Beyene, S. Parzych, S. Sharma, E. Stępień, P. Moskal, *Bio-Algorithms Med-Syst.* **19**, 87 (2023).

[20] P. Moskal, E. Czerwiński, J. Raj et al., *Nat. Commun.* **15**, 78 (2024) .

[21] P. Moskal, A. Gajos, M. Mohammed et al., *Nat. Commun.* **12**, 5658 (2021).

[22] F. Tayefi Ardebili, S. Niedźwiecki, P. Moskal, *Bio-Algorithms Med-Syst.* **19**, 132 (2023).

[23] E.C. Pratt, A. Lopez-Montes, A. Volpe et al., *Nat. Biomed. Eng.* **7**, 1028 (2023).

[24] P. Moskal, J. Baran, S. Bass et al., *Sci. Adv.* **10**, eadp2840 (2024).

[25] W.M. Steinberger, L. Mercolli, J. Breuer et al., *EJNMMI Phys.* **11**, 76 (2024).

[26] P. Moskal, E. Kubicz, G. Grudzień, E. Czerwiński, K. Dulski, B. Leszczyński, S. Niedźwiecki, E.Ł. Stępień *EJNMMI Phys.* **10**, 22 (2023).

[27] H. Karimi, P. Moskal, E.Ł. Stępień, *Sci. Rep.* **13**, 7648 (2023).

[28] S. Moyo, P. Moskal, E. Stępień, *Bio-Algorithms Med-Syst.* **18**, 163 (2022).

[29] A.V. Avachat, K.H. Mahmoud, A.G. Leja, J.J. Xu, M.A. Anastasio, M. Sivaguru, A. Di Fulvio, *Sci. Rep.* **14**, 21155 (2024).

[30] P. Moskal, E. Stępień, *Bio-Algorithms Med-Syst.* **17**, 311 (2021).

[31] K. Shibuya, H. Saito, F. Nishikido, M. Takahashi T. Yamaya, *Commun. Phys.* **3**, 173 (2020).

[32] S.D. Bass, S. Mariazzi, P. Moskal, E. Stępień, *Rev. Mod. Phys.* **95**, 021002 (2023).

[33] P. Moskal, E. Stępień, W. Mryka, I. Kadenko, N.V. Sakhno, "Cross-sections of (p,x) reactions on ^{12}C, ^{14}N and ^{16}O for ^{10,11}C production", Jagiellonian University, Kraków 2024.

[34] I.M. Kadenko, N.V. Sakhno, P. Moskal, *Bio-Algorithms Med-Syst.* **19**, 139 (2023).

[35] P. Moskal, E. Stępień, W. Mryka, I. Kadenko, N.V. Sakhno, "Cross-sections and gamma-yields in (p,x) reactions on ^{14}N and ^{16}O for ^{14,15}O production", Jagiellonian University, Kraków 2024.